Available online at www.sciencedirect.com
ScienceDirect
Surface & Coatings Technology 201 (2006) 1519–1527
SURFACE & COATINGS TECHNOLOGY
www.elsevier.com/locate/surfcoat

Determination of proper processing conditions of material surface heat treatment through finite element method

Wei Ma *, Bin Wu

Institute of Mechanics, Chinese Academy of Sciences, 15 Beisihuanxi Road, Beijing, 100080, China

Received 15 June 2005; accepted in revised form 13 February 2006
Available online 6 March 2006

Abstract

A two-dimensional model has been developed based on the experimental results of stainless steel remelting with the laminar plasma technology to investigate the transient thermo-physical characteristics of the melt pool liquids. The influence of the temperature field, temperature gradient, solidification rate and cooling rate on the processing conditions has been investigated numerically. Not only have the appropriate processing conditions been determined according to the calculations, but also they have been predicted with a criterion established based on the concept of equivalent temperature area density (ETAD) that is actually a function of the processing parameters and material properties. The comparison between the resulting conditions shows that the ETAD method can better predict the optimum condition.

Keywords: Laminar plasma technology; Thermo-physical characteristic; Remelting; Stainless steel; Equivalent temperature area density

1. Introduction

The previous studies [1,2] have demonstrated that the laminar plasma stream has a steadier flow state and a smaller axial temperature gradient than that of turbulent plasma stream, which is very important to improve the effects for material surface modification. However, the effects of gas feeding and nonstop discharge in the generating procedure often cause the irregular moving of arc root in torch channel and the super-high temperature of the plasma core also results in a large temperature gradient at generator anode exit. Therefore, it is very difficult to keep the properties of the laminar plasma stream as close to the plasma core where the heat flux density of the plasma stream varies sharply with its axial distance. When the laminar plasma technology is used to perform the surface processing of materials, the heating distance is usually in the region of 8 to 20 mm, in which, as indicated in the studies [2], the axial temperature gradient has reached the order of the 10^3 °C/mm and the features of heat flux density are not yet understood completely. Since the limitation of the testing means, an unambiguous comprehension of the laminar plasma features is almost impossible just by means of the experimental studies. However, with the help of the numerical simulation method, we can desire to get more comprehensive understanding about it.

In the last several decades, it has been paid a great attention to the problem of how to evaluate the effects of material surface processing either in laboratory investigation or in engineering application, and a large number of relevant experimental and modeling studies have been performed [3–8]. These studies principally involved the microstructure evolution of surface modified layers and the heat transfer mechanisms in heating process. Usually, it is desired from the viewpoint of engineering efficiency that the surfaces processing can produce the greatest possible depth of heat affected zone, the most perfect microstructure of surface modified layer and the smallest possible distortion of workpiece [9]. However, both the plasma processing and the laser technology must live with some problems to some extent, since there is always a clear conflict among the wish to optimize the microstructure, the need to obtain the greatest possible depth and the desire to minimize the workpiece distortion. Due to the complex of the processing conditions, it is almost impossible to resolve the problems through experimental investigations alone. Hence, it is necessary to carry out theoretical

* Corresponding author. Tel.: +86 10 82622614; fax: +86 10 62651284.
E-mail address: watwm@imech.ac.cn (W. Ma).

0257-8972/$ - see front matter © 2006 Elsevier B.V. All rights reserved.
doi:10.1016/j.surfcoat.2006.02.031

and numerical studies systematically and to establish an effective method to appraise the processing effects correctly. Obviously, the method should be based on the reasonable theoretical analysis and experimental investigation, and sufficiently consider the practicalities of the processing. Generally, the plasma processing involves much more complicated phenomena than that of laser technology owing to the influences of working gas pressures. Although a great number of modeling studies on the plasma processing have been conducted [10], there is still a great lack of the numerical simulation studies on the laminar plasma processing. Particularly, these studies hardly involve the method to predict the appropriate processing conditions correctly. Therefore, in this paper, we first establish a thermo-physical model based on the experimental observations and give relevant mathematic formulation; then study the transient characteristics of the melt pool liquids through the finite element method and find the correlations between the thermo-physical characteristics and the processing conditions; and finally establish an effective method to determine the optimum condition and present the relevant discussions. The purpose is to provide a technical assistance for the processing program improvement.

2. Experimental results

In the studies [11,12], the laminar plasma technology was used to perform the surface processing of metal and alloy. During testing, only the heating distance that was chosen as a single controlling parameter changes from 3 to 20 mm and the remaining parameters were kept constant. Fig. 1 illustrates the remelting results of stainless steel at a variable heating distance. As it is small, the groove appearances of the surface modified track develop and the smaller it is, the deeper the groove is (Fig. 1(a) and (b)). Two kinds of mechanisms may be responsible for the results: one is the gasified phenomenon of the high temperature substance induced by the plasma core and the other is the fast flow of melt pool liquid with low viscosity toward both sides of the remelting track induced by the plasma gas pressure. Further experimental results show that, when it is in the range of 10 to 15 mm, the surfaces of the remelting tracks become rather smooth as shown in Fig. 1 (c) and (d). However, when it increases to 20 mm, the melt pool is not formed on the substrate surface due to the poor heat absorbability during the remelting process (Fig. 1(e)). The fact shows that there must be a suitable heating distance matching to the optimum condition. Similarly, if other processing parameter, such as the scanning velocity, is chosen as the controlling parameter, the testing results show that it could produce same effects on the processing conditions as that of the heating distance [11].

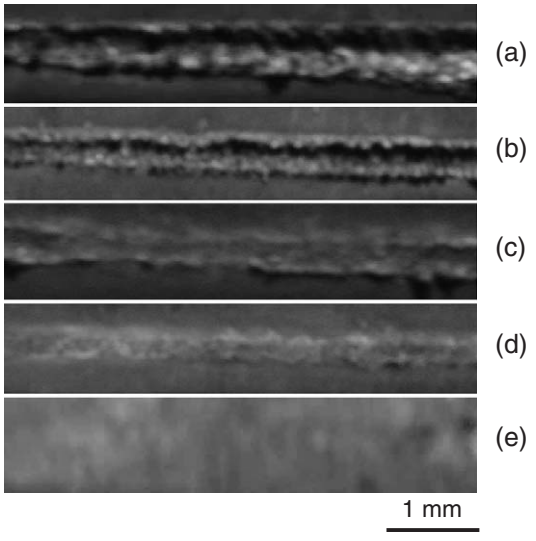

Fig. 1. The macroscopic profiles of the remelting tracks on the stainless steel surface with different heating distances: (a) 3 mm, (b) 5 mm, (c) 10 mm, (d) 15 mm and (e) 20 mm.

3. Modeling

3.1. Thermo-physical model

Fig. 2 illustrates the remelting process with the laminar plasma technology on a workpiece surface moving at a constant velocity. Three aspects are involved in the process: the first one is *the rapid heating process*, which directly associates with the thermo-physical characteristics of treated materials. The initial molten process mainly involves the state change, heat conductivity as well as heat and mass transfer, and the sequential solidification usually associates with the mechanisms of microstructure evolution, grain growth and phase transformation. These are closely related to the transient temperature field, temperature gradient, solidification rate and cooling rate of the melt pool liquids. The second is *the processing conditions*, which not only deal with many processing parameters, such as the heating distance, the scanning velocity and the input power, but also is closely related to the plasma stream features as the heat flux density and the plasma stream flow state. The third is *the properties of the surface modified layers*, which both associate with the plasma stream features and with the thermo-physical characteristics. On the one hand, the stable plasma stream flow generates the remelting tracks with good macroscopic features; on the other hand, the heat flux fluctuation in radial direction induces drastically uneven microstructure of the modified layer. Moreover, the solidification characteristics of the melt pool liquid clearly influence the mechanisms of the grain nucleation and growth. Therefore, for such a complicated process, if the major interest is focused on the prediction of the optimum condition based on the transient characteristics of the melt pool liquid and the treatment effects of the surface modified layer, some specific simplifications must be made so that a logical and feasible model can be established for the performance of finite element simulations.

The relevant assumptions for the model include:

(1) Since solidification is a transient process, the heat exchange with surrounding medium is of minor importance.

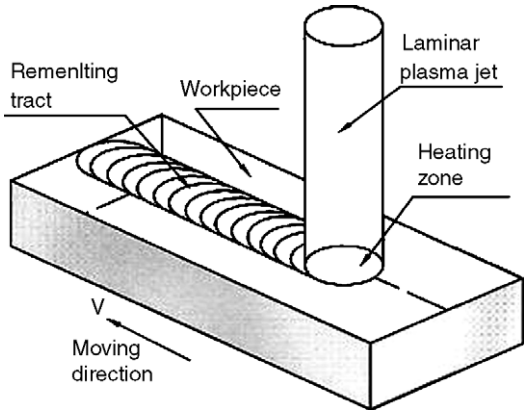

Fig. 2. Schematic diagram of the thermo-physical model.

Thus, the transient thermo-physical problem describing the process is assumed to satisfy adiabatic boundary conditions, which principally adept to the top and bottom surfaces of workpiece.

(2) As pointed out in the studies [8] that the temperature gradient in the cross section of remelting track is very larger than that in the longitudinal section, so that the heat flow is principally limited in the cross section. In addition, it is very hard to picture the difference of the transient temperature fields on two arbitrary cross sections of the track except for a limited delay in time. Therefore, we can make a hypothesis that the transient thermo-physical properties of melt pool liquid are invariable along the track longitudinal direction and only dependent on the variables in the cross section.

(3) Because that the melt pool liquid experiences large temperature fluctuation, the effects of the temperature on the material thermo-physical properties are very significant in solidification. Fig. 3 illustrates the variation of the thermo-physical properties with temperature when the temperature increases from 20 to 900 °C [13]. The relevant data when the temperature is above 900 °C are obtained by non-linear curve fitting. The resulting relations between the thermal conductivity, the specific heat and the temperature are expressed as

$$\begin{aligned} k(T) &= k_0(C_0 + C_1T + C_2T^2 \quad (T < T_{\mathrm{mel}}) \\ c(T) &= c_0(D_0 + D_1T + D_2T^2) \end{aligned} \tag{1}$$

where k_0 and c_0 are the thermal conductivity and specific heat of the substrate material at room temperature, respectively. The constants are: $C_0=0.97$, $C_1=5.85\times10^{-4}$, $C_2=4.85\times10^{-7}$, $D_0=0.99$, $D_1=4.18\times10^{-4}$ and $D_2=-1.58\times10^{-7}$. When the temperature increases above the melting point, T_{mel}, the thermal conductivity of the melt pool liquid will be further modified according to the method proposed in Ref. [7].

(4) In the remelting, the melt pool volume is quite small compared to the substrate volume due to the high concentration of plasma source on a small surface area. Moreover, the convection velocity of the melt pool liquid is much weaker than that of the heat conduction [8]. Therefore, only the effect of heat conduction is involved in the model and the convection effects are omitted, from which the loss of the heat energy is offset by introducing a modified heat conductivity [7]. Usually, the effective heat conductivity is at least twice the stationary melt liquid conductivity [4] and can be represented as

$$\kappa^*(T) = \eta\kappa(T_{\mathrm{mel}}) \quad (T > T_{\mathrm{mel}}) \tag{2}$$

where κ^* is modified heat conductivity and η is a dimensionless correction coefficient.

(5) In the model, the heat flux intensity of the plasma source, $Q(x,t)$, is modeled as a Gaussian distribution with regard to the spatial coordinate x and time t:

$$Q(x,t) = \frac{\beta Q_0(d,V,P)}{\omega} \mathrm{e}^{-((x-a)/a_0)^2} \left[\mathrm{e}^{-((t/t_s)-(a_0/Vt))^2} - \mathrm{e}^{-(a_0/Vt)^2}\right], \ (-a < x < a) \tag{3}$$

where $a^2=a_0^2-(a_0-Vt)^2$. V, t_s and a_0 are the scanning velocity, scanning time and plasma stream radii,

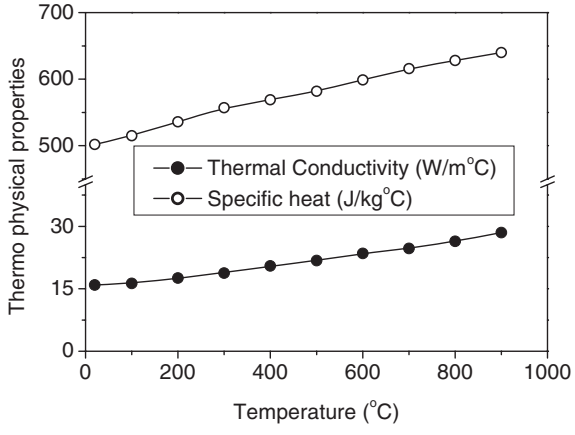

Fig. 3. The connections between the thermo-physical properties of material and the temperature.

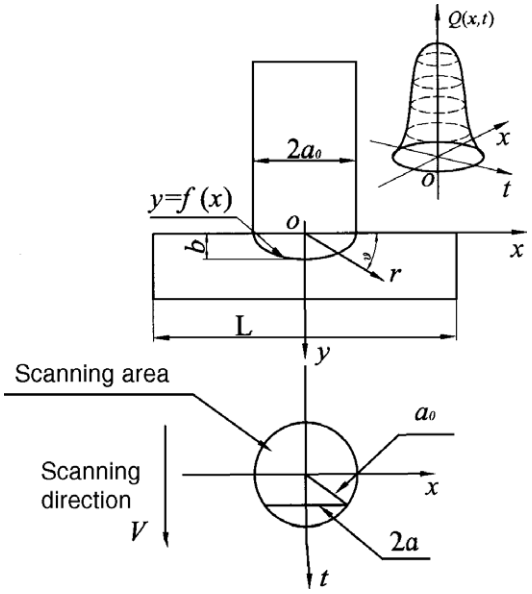

Fig. 4. The two-dimensional model for the finite element calculation.

respectively (Fig. 4). ω is a modified coefficient, and β and $Q_0(d,V,P)$ are the absorption coefficient and the intensity factor of heat flux density of plasma source, respectively. The dependency of the absorption coefficient β on the temperature is taken into account in the model. When the temperature varies from room temperature to melting point, for simplicity, a proportion relation between the absorption coefficient and temperature is adopted. When the temperatures exceed the melting point, its value is fixed in 34% [6,14]. The intensity factor $Q_0(d, V,P)$ is assumed as the function of the heating distance d, scanning velocity V and input power P, and can be expressed in separation form

$$Q_0(d,V,P) = \frac{2Q_1(d)Q_2(V)Q_3(P)}{\pi a_0^2} \tag{4}$$

where the three functions $Q_1(d)$, $Q_2(V)$ and $Q_3(P)$ can be determined from the experimental results, respectively [2]. Fig. 5 illustrates the dependences of these functions on the processing parameters. It should be noted that, when the heat distance is less than the 40 mm, the heat flux density is strongly dependent on the heat distance, but is almost not related to the input power. Because that the remelting distances are usually in the region of 8 to 20 mm, the influences of the input power on the heat flux density are neglected in the model. Therefore, the power factor $Q_3(P)$ is setting to be unit in expression (4). By the exponential decay fit of second orders, the distance factor $Q_1(d)$ is determined as

$$Q_1(d) = A_0 + A_1 e^{-\lambda_1 d} + A_2 e^{-\lambda_2 d^2} \tag{5}$$

where $A_0 = -5.27\times10^6$, $A_1 = 1.56\times10^7$, $A_2 = 2.27\times10^7$, $\lambda_1 = 2.19$ and $\lambda_2 = -69.58$. In Fig. 5, the connection between the heat flux density and the scanning velocity is also illustrated when the heat distance is fixed at 10 mm and the input power is equal to 9 kW. For simplicity, a polynomial fit is adopted to obtain the velocity factor as follows

$$Q_2(V) = B_0 + B_1 V + B_2 V^2 \tag{6}$$

where $B_0 = 5.91\times10^7$, $B_1 = -2.32\times10^5$ and $B_2 = 2.62\times10^2$.

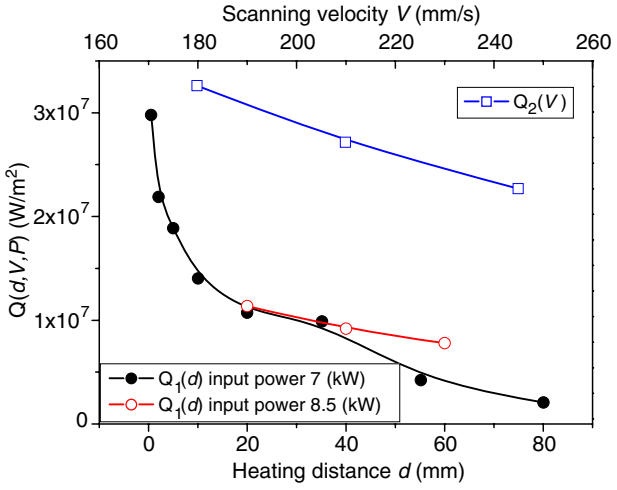

Fig. 5. The relations of the heat flux density factors, $Q(d)$ and $Q(V)$ versus the heat distance and the scanning velocity.

3.2. Mathematical formulation

The above discussion shows that the thermal analysis of the remelting process can be conducted by resolving a two-dimensional initial-boundary value problem of heat conductivity. Based on the Fourier law [15], the heat conduction governing equations are expressed as follows:

$$\nabla\left[k\left(T_n^{(m)}\right)\nabla T_n^{(m)}(x,y,t)\right] = \rho c\left(T_n^{(m)}\right)\frac{\partial T_n^{(m)}(x,y,t)}{\partial t} \tag{7}$$

where x and y are the horizontal and vertical coordinates as shown in Fig. 4 and $\nabla = (\partial/\partial x)i + (\partial/\partial y)j$ is the Hamilton operator. i and j are the unit vectors of the coordinates x and y, respectively. $T_n^{(m)}(x,y,t)$ $(m = I\sim IV)$ are the temperature fields of the four stages corresponding to the pre-melting, melting, solidifying and post-solidifying, respectively. The subscript $n = l, s$ represent the liquid and solid phases, respectively. ρ is the density. At present, the influences of density difference between the liquid and solid on the melt pool substances are omitted and the density of the solid phase is adopted in the model. The initial condition is $T_n^{(I)}(x,y,t)_{t=0} = T_0$, where T_0 is the room temperature. Considering the transient features of the remelting procedures, the governing Eq. (7) satisfies the insulated boundary conditions as follows

$$\kappa\left(T_n^{(m)}\right)\frac{\partial T_n^{(m)}(x,y,t)}{\partial \varsigma} = \begin{cases} Q(x,t) & |x| < 2a,\ y = 0, \varsigma = x \\ 0 & |x| > 2a,\ y = 0, \varsigma = x \\ 0 & y = h,\ \varsigma = x \\ 0 & x = 0,\ L,\ \varsigma = y \end{cases} \tag{8}$$

where $\kappa(T)$ is the thermal diffusivity of substance materials.

The energy balance condition and the temperature continuous condition at the liquid/solid interface are given in forms

$$\left[1 + \left(\frac{\partial f}{\partial x}\right)^2\right]\left[k_s\frac{\partial T_s^{(m)}}{\partial y} - k_l\frac{\partial T_l^{(m)}}{\partial y}\right] = \rho L\frac{\partial f}{\partial t};$$
$$T_s^{(m)}(x,y,t)|_{y=f(x,t)} = T_l^{(m)}(x,y,t)|_{y=f(x,t)} = T_{mel};\quad (m = I\sim IV) \tag{9}$$

where L is the latent heat of melting/solidification per unit mass and $y = f(x,t)$ is the location function of the liquid/solid interface. In the pre-melting stage I and post-solidifying stage IV, only heat conduction procedure take place in the homogeneous medium comprising of identical solid phase, but in the melting stage II and solidifying stage III, the heat conduction procedures are accompanied with state change.

3.3. Finite element formulation

Based on the Galerkin's weighted residual methods, the weak form of the heat conduction problems (7) and (8) is given as [16]

$$\int_\Omega \nabla^T w_j k(T)\nabla T \mathrm{d}\Omega - \int_{\Gamma_q} w_j Q \mathrm{d}\Gamma - \int_{\Gamma_T} w_j k(T)\frac{\partial T}{\partial n}\mathrm{d}\Gamma + \int_\Omega w_j \rho c(T)\frac{\partial T}{\partial t}\mathrm{d}\Omega = 0 \tag{10}$$

where w_j ($j=1, 2, \ldots, n$) is a set of arbitrarily functions satisfying automatically the natural boundary conditions. Along the boundary Γ_q, the heat source $Q(x,t)$ is prescribed by the relation (3). Moreover, if the temperature distribution is restricted so as to satisfy the forced boundary condition (8), the third term in Eq. (10) is identical to zero. If the solution of temperature distribution $T(x,y,t)$ is sought in the approximate form

$$T = \sum_{i=1}^{n} N_i(x,y)T_i(t) \tag{11}$$

where $T_i(t)$ and $N_i(x,y)$ are, respectively, the functions of time and the form functions that are only related to the spatial coordinates. From the relation (1), we can further determine the thermo-physical properties $k(T)$ and $c(T)$ as follows

$$\begin{aligned} k(T) &= \eta_0 + \eta_1\sum_{k=1}^{n} N_k T_k + \eta_2\left(\sum_{k=1}^{n} N_k T_k\right)^2 \\ c(T) &= \xi_0 + \xi_1\sum_{k=1}^{n} N_k T_k + \xi_2\left(\sum_{k=1}^{n} N_k T_k\right)^2 \end{aligned} \tag{12}$$

where constants η_i and ξ_i ($i=0, 1, 2$) can be determined from the relation (1). If setting $w_j=N_j$, we have immediately a set of equations in the form

$$[K_{ij}]\{T_j\} + [C_{ij}]\left\{\frac{\mathrm{d}T_j}{\mathrm{d}t}\right\} + [Q_j] = 0 \qquad (j = 1\cdots n) \tag{13}$$

with

$$K_{ij} = \int_\Omega \nabla^T w_j k(T)\nabla T \mathrm{d}\Omega = K_{ij}^{(0)} + K_{ijk}^{(1)} + K_{ijkl}^{(2)}$$

$$K_{ij}^{(0)} = \int_\Omega \left[\frac{\partial N_j}{\partial x}\left(\eta_0\frac{\partial N_i}{\partial x}\right) + \frac{\partial N_j}{\partial y}\left(\eta_0\frac{\partial N_i}{\partial y}\right)\right]\mathrm{d}\Omega$$

$$K_{ijk}^{(1)} = \left\{\sum_{k=1}^{n}\int_\Omega \left[\frac{\partial N_j}{\partial x}\left(\eta_1 N_k\frac{\partial N_i}{\partial x}\right) + \frac{\partial N_j}{\partial y}\left(\eta_1 N_k\frac{\partial N_i}{\partial y}\right)\right]\mathrm{d}\Omega\right\}T_k$$

$$K_{ijkl}^{(2)} = \left\{\sum_{l=1}^{n}\sum_{k=1}^{n}\int_\Omega \left[\frac{\partial N_j}{\partial x}\left(\eta_2 N_k N_l\frac{\partial N_i}{\partial x}\right) + \frac{\partial N_j}{\partial y}\left(\eta_2 N_k N_l\frac{\partial N_i}{\partial y}\right)\right]\mathrm{d}\Omega\right\}T_k T_l$$

$$C_{ij} = \int_\Omega w_j \rho c(T)\frac{\partial T}{\partial t}\mathrm{d}\Omega = C_{ij}^0 + C_{ijk}^1 + C_{ijkl}^2$$

$$C_{ij}^{(0)} = \int_\Omega N_j(\xi_0 N_i)\mathrm{d}\Omega$$

$$C_{ijk}^{(1)} = \left[\sum_{k=1}^{n}\int_\Omega N_j(\xi_1 N_k N_i)\mathrm{d}\Omega\right]T_k$$

$$C_{ijkl}^{(2)} = \left[\sum_{l=1}^{n}\sum_{k=1}^{n}\int_\Omega N_j(\xi_2 N_k N_l N_i)\mathrm{d}\Omega\right]T_k T_l$$

$$Q_j = -\int_{\Gamma_q} w_j Q \mathrm{d}\Gamma = -\int_{\Gamma_q} N_j Q \mathrm{d}\Gamma \tag{14}$$

Similarly, the weighted residual approximation is also applied to the discretization in time of the initial-boundary value problems (7) and (8). In each interval, we assume that the temperature $T(x,y,t)$ varies with time according to a linear regulation

$$T_i(t) = T_m + \frac{t}{\Delta t}(T_{m+1} - T_m) \tag{15}$$

with $\tau=t-t_m$. Thus, we can give the approximate form of Eq. (13) with a weighted residual function, $W(\tau)$, as follows

$$\int_0^{\Delta t} W(t)([C_{ij}]\{\dot{T}_j\} + [K_{ij}]T_j + [Q_j])\mathrm{d}\tau = 0 \tag{15}$$

Introducing a weighted parameter given by

$$\theta = \frac{1}{\Delta t}\frac{\int_0^{\Delta t} W\tau \mathrm{d}\tau}{\int_0^{\Delta t} W \mathrm{d}\tau} \tag{16}$$

and an average value of Q_j given by

$$Q_{ij} = \frac{\int_0^{\Delta t} WQ_j \mathrm{d}\tau}{\int_0^{\Delta t} W \mathrm{d}\tau} \tag{17}$$

Eq. (15) can be immediately rewritten as

$$T_{m+1} = ([C_{ij}] + \theta\Delta t[K_{ij}])^{-1}(([C_{ij}] - (1-\theta)\Delta t[K_{ij}])T_m - \Delta t[Q_{ij}]) \tag{18}$$

from the equation an approximation for T_{m+1} at time $t=t_m+\Delta t$ is calculated based on the value T_m at time t_m. Here, the initial value T_0 of T_m as a known parameter is prescribed.

Since the plasma source and the substrate geometries have a common symmetric axis, the intersection between the symmetric axis and the top boundary of the substrate is taken as the

Table 1
Numerical values used for the calculation in this study

Property	Symbol	Value (unit)
Thermal conductivity	k_0	15.9 W/m °C
Specific heat	c_0	502 J/kg °C
Scanning time	t_s	1.25 s
Absorptive coefficient	β	22–30%
Plasma stream radii	a_0	3 mm
Thermal conductivity modified coefficient	η	2.5
Melt point	T_{mel}	1400 °C
Heat flux density modified coefficient	ω	1.56
Room temperature	T_0	20 °C
Area modified coefficient	S_0	60 mm^2

origin of the coordinate system as shown in Fig. 4. During remelting, the origin point is also the matter point to be molten firstly and the peak temperatures to appear. For simplicity, half of the actual problem is modeled with the adiabatic boundary along the symmetry axis. The related parameters in the calculation are given in Table 1.

4. Simulation results and discussion

4.1. Transient thermo-physical characteristics

It is necessary to understand the temperature distribution of the melt pool liquids in order to evaluate the effects of material surface treatment. Fig. 6 illustrates the variations of the peak temperatures with time in the remelting. When the heating distance is equal to 3 mm, the largest peak temperature exceeds 3800 °C (Fig. 6(a)). As it increases, the largest peak temperature decreases quickly. Particularly, it should be noted that, as it increases from 5 to 10 mm, the largest reduction arrives at 1050 °C. In addition, the time when the largest peak temperature is reached is about 0.8 s, which implies that the melt pool area extends to its maximum nearly at the same time and is independent of the heating distance. Fig. 6(b) illustrates the peak temperature variation with time when the scanning velocity is chosen as the controlling parameter. As it decreases, the largest peak temperatures and the heating intervals gradually increase and no abrupt change is observed. Moreover, that the largest peak temperature is not reached concurrently means the largest melt pool area arrived at different time. Clearly, the different effects of the two parameters on the temperature fields are due to the fact that the heat flux density of the plasma source associates with them in completely different ways. During the heating process, the variation of the heating distance results in the great change of the heat flux density, but the variation of the scanning velocity only changes the heating intervals.

The temperature gradient is an important factor influencing the microstructure of surface modified layers [17]. Fig. 7 illustrates the influences of the processing parameters on the temperature gradient. Similar to the temperature distribution, it is strongly associated with the heating distance but slightly with the scanning velocity. This is because that the heat flux density of the plasma stream evidently varies with the heating distance when it is less than 20 mm. At small heating distance, high heat absorption of the plasma stream make the melt pool liquid

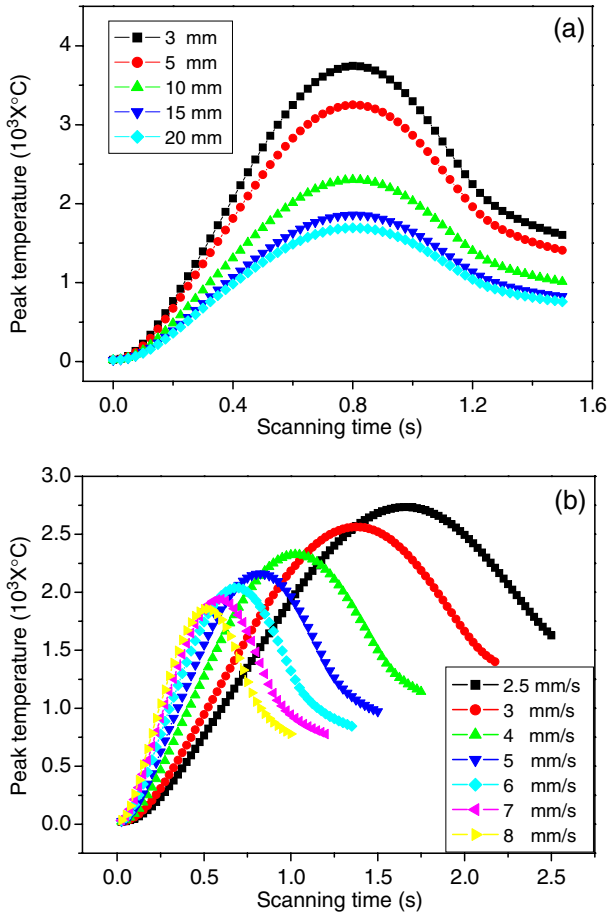

Fig. 6. The variations of the peak temperatures with time: (a) the heat distance and (b) the scanning velocity.

obtain more thermal energy and develop large temperature gradient; whereas, as it increases, poor heat absorption results in small temperature gradient. Moreover, along the directions with different radiant angles $\theta = 0°$, 45° and 90° on the pool transect plane (Fig. 4), the gradient curves consisting of two linear segments have evident geometric similarity with each other

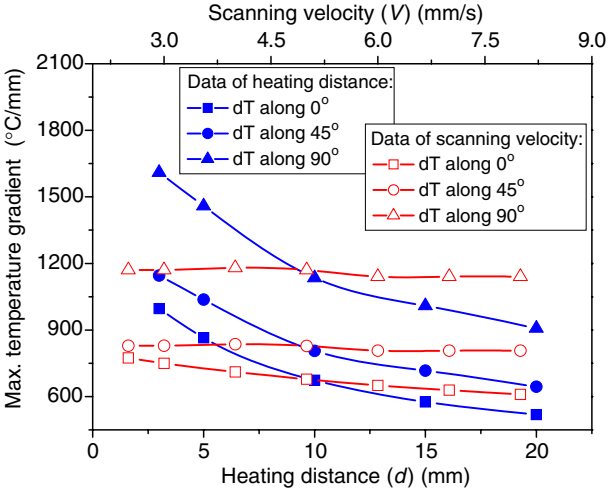

Fig. 7. The maximum temperature gradients related to the different processing parameters along three radials with the radiant angles: $\theta = 0°$, $\theta = 45°$ and $\theta = 90°$.

except for the different magnitudes. The inflexions appear at the heating distance of 10 mm and the increasing rates are averagely equal to 112 °C/mm and 248 °C/mm, respectively. Since the temperature gradient is scarcely affected by the scanning velocity, and in view of the effects of the temperature gradient on the microstructure, a correct choice for a heating distance, which should be in the region of 10 mm to 15 mm, will be more important than that for a scanning velocity.

In the remelting process, the microstructure evolution is restricted to follow closely the heat flow, which is perpendicular to the moving liquid/solid interface. Therefore, the crystal growths usually take place ahead of the solidification fronts. Thus, it can be desire to produce a fine microstructure with small grain scales by controlling the solidification mechanisms. Fig. 8(a) shows the dependences of the maximum solidification rate on the heating distance. Inside the melt pool, the solidification rates reach their peak values at the heating distance of 11 mm. When it decreases, the solidification rates initially decrease from the peak values and then increase suddenly after reaching their valley values. It is the gasification of the melt pool liquid that dissipates a large amount of plasma heat energy, which makes the solidification rates enhance quickly. On the melt pool surface, a high temperature gas boundary layer formed by the plasma gas, which considerably obstructed the heat convection between the melt pool liquid and

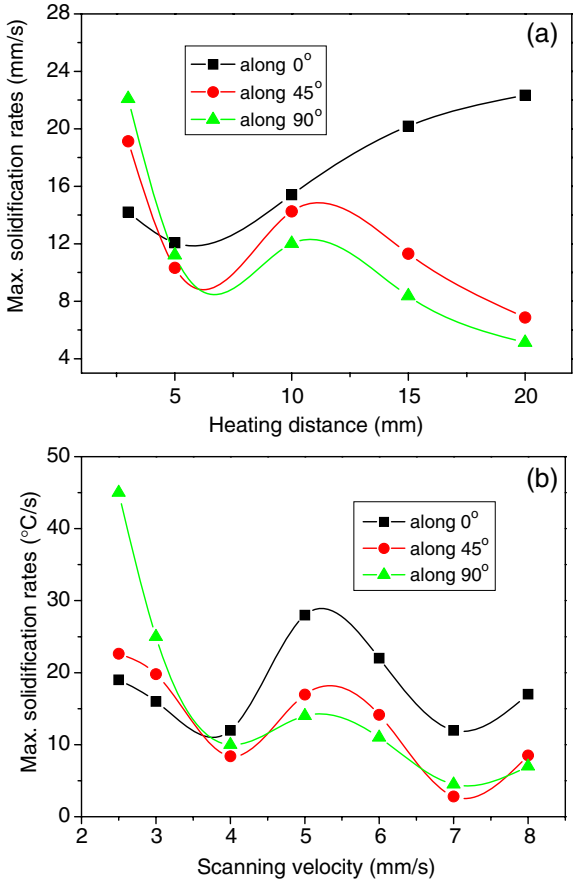

Fig. 8. The solidification rates of the melt pool liquids: (a) the different heating distances and (b) the scanning velocity.

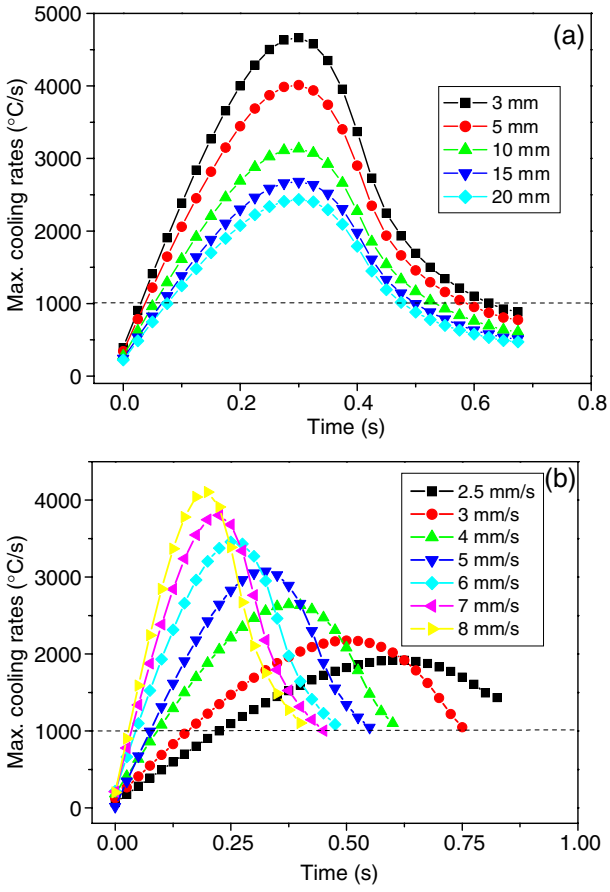

Fig. 9. The cooling rates of the melt pool liquids: (a) the different heating distances and (b) the scanning velocity.

the surrounding medium when the heating distance is small. However, when the heating distance increases, this thermal barrier function of the gas boundary layer rapidly becomes powerless, which results in the quick thermal dissipation and the solidification rates raise continually. Fig. 8(b) illustrates the variations of the maximum solidification rate with the scanning velocities when the heating distance is fixed on 10 mm. As seen in the plot, when the scanning velocity approaches to 5.5 mm/s, it arrives at the peak values and the differences between inside the melt pool and on the pool surface are no longer existed. This implies that the influence of the scanning velocity, when it varies from 4 mm/s to 8 mm/s, on the solidification rate is minor important. In fact, the heating distance of 10 mm still plays a crucial role. Based on the calculations, it can conclude that, in order to ensure the solidification rates as high as possible, the appropriate heating distance should be selected in the region of 8 mm to 13 mm, and the corresponding scanning velocity should be in the region of 4 mm/s to 6 mm/s.

It is well known that the crystal nucleation mechanisms closely related to the cooling rate. High cooling rate of the melt pool liquids results in a high nucleation density, but a short growth interval for the grains, which is great helpful to the development of a fine microstructure in the surface modified layers [18]. From Fig. 9, we can see that, once the melt pool liquid starts to cool, the peak cooling rate exceeds 1000 °C/s

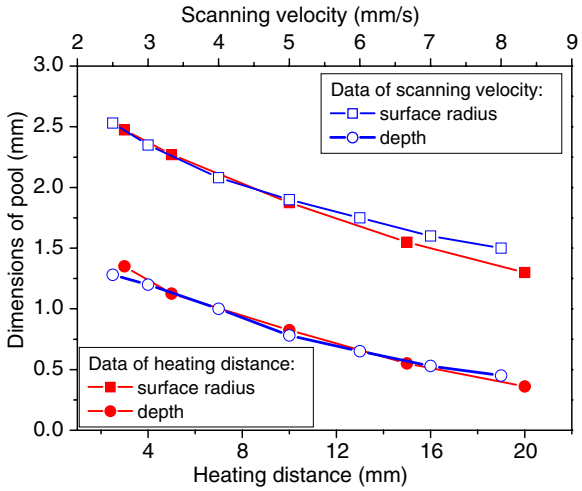

Fig. 10. The relations between the dimensions of the melt pools and the processing parameters.

very rapidly and is independent of the processing parameters. Usually, the cooling of the melt pool liquid starts roughly at the time when the melt pool reaches its largest area; in other words, it is almost simultaneous with the solidification. This fact shows that the laminar plasma remelting processing can produce a quite high cooling rate in the melt pool liquid during the solidification.

4.2. Evaluation of the processing conditions

It has seen that the microstructures of the surface modified layers, the transient thermo-physical characteristics of the melt pool liquids and the dimensions of the melt pools are closely dependent on the processing parameters. In order to achieve the best results, it is necessary to select the appropriate processing parameters. However, since there are many parameters involved in the remelting, which are strongly coupled with each other, making the optimal selection needs to have a wholly theoretical and experimental consideration of the complex procedures. That is to say, the resulting compromise in the selection of the parameters should involve in all ways including the satisfying microstructures that can meet the specific requirements in application, the sufficient large areas of the melt pools that ensure the enough high efficiency and the acceptance of a level of distortion that the treated component has to be tolerated. Therefore, in order to determine the optimum condition, a dimensionless parameter called as the equivalent temperature area density (ETAD) is suggested:

$$F(d,V,Q)=\frac{T_e}{A_p}\{P(d,V,Q);\ M(\kappa,C,\beta)\} \tag{19}$$

where $P(d,V,Q)$ and $M(\kappa,C,\beta)$ are, respectively, the functions of the processing parameters and the material thermo-physical properties. d is the heating distance. $T_e=(T_{mpt}-T_{mel})/T_{mel}$ is the dimensionless equivalent temperature of the melt pool liquids, in which T_{mpt} is the maximum peak temperature. $A_p=\pi ab/(2S_0)$ is the dimensionless area of the melt pool if its shape is assumed to be a half ellipse as shown in Fig. 4. S_0 is a prescribed area parameter comprising of sample characteristic lengths. These quantities are related to the thermo-physical properties of the substrate materials, the geometrical features of the melt pools and the processing parameters. Hence, the parameter, $F(d,V,Q)$, is actually a universal function of the processing parameter function $P(d,V,Q)$ and the material property function $M(\kappa,C,\beta)$. Theoretically, the minima of the function $F(d,V,Q)$ determined according to the extremum conditions, $\partial F(d,V,Q)/\partial V=0$ and $\partial F(d,V,Q)/\partial d=0$, are supposed to be the appropriate processing conditions. Therefore, as a criterion, it can be used to determine the optimum condition, which can meet the needs to obtain the greatest possible economic efficiency.

Fig. 10 illustrates the dependence of the melt pool dimensions on the processing parameters. It reveals that, when these parameters decrease, the widths and depths expand, respectively, from 3 to 5 mm and from 0.4 to 1.3 mm according to approximate linear relations. Based on the results, the values of the ETAD can be determined. As seen in Fig. 11, it is quite sensitive to the heating distance but insensitive to the scanning velocity. When the heating distance increases from 3 mm to 20 mm, its value initially decreases from a high level of about 47 and then increases slightly after reaching its minimum at the 12.5 mm. However, when the scanning velocity increases from 2.5 mm/s to 8 mm/s, the steep change of its value is not observed even though it reaches a minimum at the scanning velocity of about 5 mm/s. Clearly, these results are induced by the common influences of the peak temperatures of the melt pool liquid and the melt pool dimensions. Furthermore, we have noted that there is always a minimum on each ETAD curve, which is supposed to represent the optimum condition theoretically. Therefore, for the laminar plasma remelting, the appropriate heating distances should be in the region of 9–13 mm and the scanning velocities in the region of 3–7 mm/s, which is in agreement with the experimental observations very well.

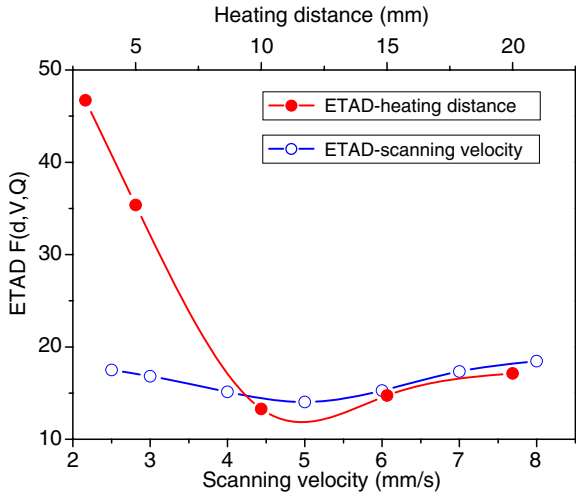

Fig. 11. The distribution of the ETAD as a function of the processing parameters.

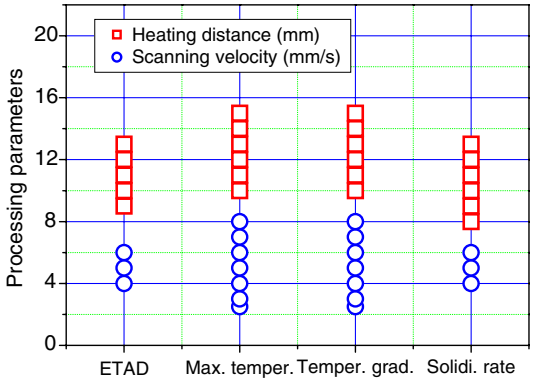

Fig. 12. The comparison between different processing conditions obtained with varied methods.

As seen above, the function ETAD reveals the dependence of the processing conditions on the thermo-physical characteristics of the melt pool liquid and establishes the connection between the processing conditions and the treatment effects. Moreover, it can also predict the optimum condition when its minimum is determined. In order to compare the condition with those obtained from the calculations of the thermo-physical characteristics, a schematic representation of the relevant results is given in Fig. 12. It can see that the former is almost covered by the latter, which suggests that the ETAD method is indeed a more effective way to determine the optimum condition for the laminar plasma processing.

5. Conclusion

Based on the results of the laminar plasma remelting of the stainless steel, a thermo-physical plane strain model has been established in order to study the transient solidification mechanisms of the melt pool liquids and the processing conditions. The correlations between the transient characteristics in the melt pool liquids, the geometries of the melt pools and the processing parameters are studied by the finite element simulations. On the one hand, the appropriate processing conditions are determined based on the transient characteristics of the melt pool liquids. On the other hand, a dimensionless parameter ETAD is introduced as a criterion in order to judge the processing conditions. This parameter also establishes the connections among the processing parameters, the thermo-physical properties and geometries of the melt pools and considers the dependence of the material on the current temperatures. According to the extremum conditions, the optimum condition can be determined. The comparison among the resulting conditions shows that the condition determined by ETAD is more appropriate than others for the remelting processing.

Acknowledgement

Our great thanks are due to The National Natural Sciences Foundation of China (No. 10275085) for supporting this work.

References

[1] W. Ma, W.X. Pan, C.K. Wu, Surf. Coat. Technol. 191 (2005) 166.
[2] W.X. Pan, W.H. Zhang, W. Ma, C.K. Wu, Plasma Chem. Plasma Process. 22 (2) (2002) 271.
[3] A.P. Markwood, R.C. Crafer, Opt. Laser Technol. 37 (2) (2005) 99.
[4] E. Toyserkani, A. Khajepour, S. Corbin, Opt. Lasers Eng. 41 (6) (2004) 849.
[5] Y. Fu, A. Loredo, B. Martin, A.B. Vannes, J. Mater. Process. Technol. 128 (2002) 106.
[6] G. Zhao, C. Cho, J.D. Kim, Int. J. Mech. Sci. 45 (2003) 777.
[7] C. Lampa, A.F.H. Kaplan, J. Powell, C. Magnusson, J. Phys., D, Appl. Phys. 30 (1997) 1293.
[8] J.D. Kem, Y. Peng, J. Mater. Process. Technol. 104 (2000) 284.
[9] A.J. Fletcher, Thermal Stress and Strain Generation in the Heat Treatment, Elsevier Science Publishers LTD, London, England, 1989.
[10] E. Pfender, Thin Solid Films 238 (1994) 228.
[11] W. Ma, Q.X. Fei, W.X. Pan, C.K. Wu, Appl. Surf. Sci. 252 (2006) 3541.
[12] W. Ma, Q.X. Fei, W.X. Pan, C.K. Wu, The 7th APCPST (Asia Pacific Conference on Plasma Science and Technology) & 17th SPSM (Symposium on Plasma Science for Materials). June 29th–July 2nd, 2004, Fukuoka city, Japan. 119, 2004.
[13] Practical Handbook of Engineering Materials, vol. 3, Chinese Standard Press, 1989 (in Chinese).
[14] L. Han, F.W. Liou, Int. J. Heat Mass Transfer 47 (2004) 4385.
[15] H.S. Carslaw, J.C. Jaeger, Conduction of Heat in Solids, Oxford University Press, Amen House, London, 1959.
[16] O.C. Zienkiewicz, R.L. Taylor, Fifth edition, The Finite Element Method, vol. 1, Butterworth-Heinemann, England, 2000.
[17] W. Ma, Appl. Surf. Sci. (in press) (Available online at www.sciencedirect.com).
[18] M. Gremaud, D.R. Allen, M. Rappaz, J.H. Perepezko, Acta Metall. Mater. 44 (1996) 2669.